STATE OF THE ART: WP6 ANDDURO

Abstract

The present document concerns the State of the Art of the WP6 ANDDURO: Management of Processes – Development of in-situ control systems

DATE: 11/01/2018

REFERENCE: LIV-M-031-L35-357-V0

Author(s)	*Function(s) & name(s)*	*Post-Doc Position*	*Robin KROMER*
Checker(s)	*Function(s) & name(s)*	*WP6 Manager* *Project Leader*	*Jean-Marc AGULLO* *Céline LARIGNON*
Approver	*Function & name*	*Materials Department Manager*	*Simon PERUSIN*

Table of Contents

Revision Table

Issue	Date	modified §	Evolution summary	Modified by
0	30/04/18	R. KROMER	Creation	

1 Introduction

1.1 Goal

This document defines a state of the art about in-situ characterization systems developed since 2010. Few scientific results were presented in measurement science for real-time control of additive manufacturing powder bed fusion processes. The aim is to present and evaluate the advantages and disadvantages of each system worldwide. Different technologies are presented. A new system is proposed to obtain a real-time evaluation of the material integrity during the process of additive manufacturing by selective laser melting of metal powder.

1.2 Motivation

As part of the ANDDURO project within IRT Saint Exupéry, an experimental bench is being developed in order to understand the physical mechanisms, specifically the phenomena generating defects, occurring during laser-powder interactions (absorption, heating, fusion, vaporization, spattering). A wide range of parameters influence the health of SLM (Selective Laser Melting) manufactured parts at various scales, such as photonic absorption, processing strategy, powder bed layering, and process environments. Some parameters are controllable but can vary over time (physical instabilities) and intrinsic or extrinsic variables can evolve. While current AM (additive manufacturing) machine tool are greatly improved from early versions, many of the same problems identified by early researchers in 1980s (porosity, cracking, thermal management, material supply) persist. This is largely attributable to a lack of in-process monitoring and closed loop control algorithms used to manage machine operation. In addition, post-mortem material inspection is not always simple depending on the geometry and the materials. This is why in-situ analyzes are required for the manufacture of laser powder-bed fusion such as used within conventional machine tools. Data (force, position, acoustic sensing) gathered here in-process is now commonly processed in-real time to affect an “on-the-fly” response in machining strategy. The quality of the part could be evaluated or an in-situ control could be envisaged in order to compensate the spatio-temporal deviations for AM. A new range of sensors and means of incorporating them into additive tools will be required.

An open-architecture bench is currently developed and it will permit to produce demonstrable technologies, capable of acquiring useful data for informing capability without the need of ex-situ analysis. However, sensors are normally attributed for a specific

application, direct measurement and in a specific environment. Sensor technologies are hence calibrated into the system and standard errors deviation quantified. High-speed powder-bed displacement will be possible and direct visualization and characterization of the melt pool is envisaged. Incorporation in additive tools would suggest signal deteriorations, but it will be quantified with this innovative structure. Furthermore, indirect measurement monitoring is chosen in AM processes. However, setting up a process means to link the input parameters (e.g. process parameters and part geometry) to output parameters (part properties, surface quality). Information (such as process emissions, melt pool size, melt pool dynamics, and temperature distribution) can be used to find some correlation for health material evaluation (Figure 1). For instance, meta-models can be developed using the input parameters, the in-process signals and part properties. However, in-process monitoring seems not clear yet. The lab-bench will permit a direct visualization for the expert associated to the acquired data. It will then be possible to create closed-loop feedback depending on physics laws and expertise.

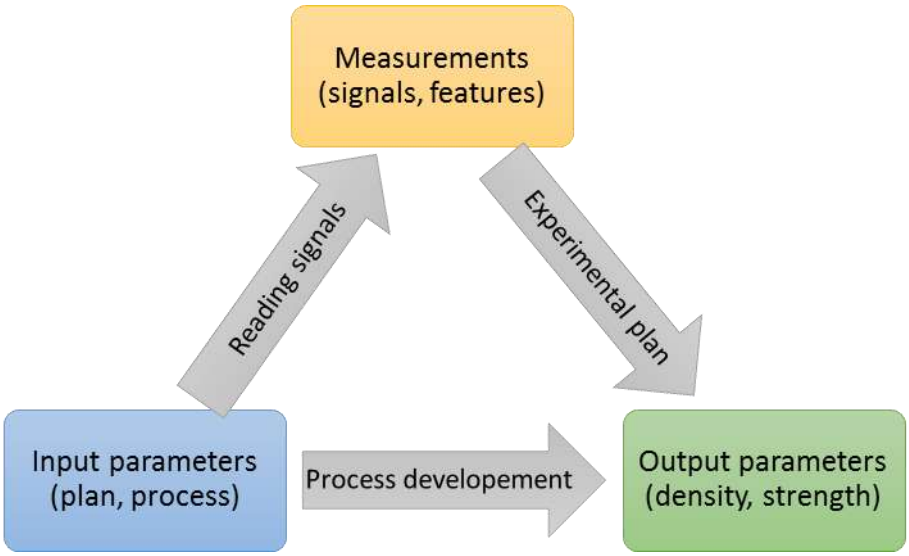

Figure 1: Learning reading strategy for health material evaluation

2 State of the art

2.1 Abbreviations

AM: Additive Manufacturing

LDED: Laser Directed Energy Deposition

EBAM: Electron Beam Additive Manufacturing

LPBF: Laser Powder Bed Fusion

SLM: Selective Laser Melting

SLS: Selective Laser Sintering

NIST: National Institute of Standards and Technologies

HAZ: Heated Affected Zone

IR: Infra-Red

PH: Precipitation Hardening

RTD: Resistance Thermal Detector

2.2 Introduction

In recent years, additive manufacturing (AM) has seen a large growth in utilization. The adoption of AM is directly related to interest in producing parts with higher complexity than feasible using traditional manufacturing processes. It allows parts to be built from the ground producing the capability for internal structures and geometries that would be otherwise unattainable. AM methods such as laser directed energy deposition (LDED) and electron beam additive manufacturing (EBAM) methods allow for larger parts to be made much faster, but at the cost of dimensional accuracy. Parts made using LDED or EBAM are typically described as near-net shape parts, describing the frequent need for post-build machining. In contrast, laser powder bed fusion (LPBF) is capable of constructing parts within tighter tolerances than previously mentioned AM methods, but it is typically limited to a smaller build volume. It has become an extremely active research field.

LPBF systems are composed of both powder delivery and energy delivery systems [1]. The powder delivery system comprises a supply powder system, a recoater to create the powder layer, and a piston that holds the fabricated part. The energy delivery system is made up of a laser (usually a single-mode continuous-wave Ytterbium fiber laser operating at 1070 nm wavelength) and a scanner system with optics that enable the delivery of a focused spot to all points of the build platform. A flow of gas (usually nitrogen or argon) passes over the powder bed with the intention to protect the part from oxygen and to clear any “spatter” and metal fumes that are created due to the laser path. Some systems have an in situ process-monitoring capability that can image the melt pool using a high-speed camera or a temperature sensor that is in-line with the laser system.

During production, the laser executes a scanning or exposure strategy. The strategies associated with the laser path are characterized by the length, direction, and separation

(hatch spacing) of neighboring scan vectors. A detailed discussion of scanning strategies is beyond the scope of this paper, but a list of scanning strategies has been compiled by Yeung et al. [2]. A physical understanding of the metal powder bed fusion process can provide insight into performance margins and their sensitivities to process parameters. Thus, a physical understanding of the process is an essential element of part qualification, especially for defects analysis. Indeed, despite significant technological advances, the defect ratios are still high with respect to more conventional production systems. To face this issue, the development of process monitoring methodologies based on in-situ sensing as well as novel feedback control strategies is required [3]. Such an understanding should enable a control of the process and a “control in-situ” could be developed.

In recent years, the state of the art in LPBF has improved to the point where is transforming from a rapid-prototyping technology to a production technology. Parts can be fabricated at near full density with mechanical properties that are similar to produced metals. A physical understanding is yet necessary for insight performance margins, uncertainties and the sensitivities. Modeling and simulating of the AM process provides a mechanism to develop this understanding. It has the potential to provide the next step in such voxel by voxel control of the process. Simulations of the additive manufacturing process are in development to evaluate the multi-physic and multi-scale modeling. However, experimental inspections are required to validate the models: thermal, thermomechanical, residual stress, laser-powder interaction, etc [4-7].

Although the powder bed fusion process is conceptually simple, the underlying physics is complex and covers a broad range of time and length scales. Laser beam interaction and powder layer thicknesses, laser speeds are about 10 J, 10 μm and 1 m/s respectively. On the other hand, parts are many cubic centimeters in dimension and build times can be hours, days, even weeks. Further, the process involves around 130 parameters that could affect the quality of the final part [8]. The main parameters such as the laser power, laser spot speed, and beam size control the length, width, and depth of the melt pool, are generally expressed by the energy density Ed=P/(v.s.t) [9]. Generally speaking, it is desirable to maintain constant or controlled melt pool geometry during a build. However, others uncontrollable properties, such as powder bed density or gas environment, fluctuates during the process and limit the continuous melt flow.

However, because the thermal boundary conditions change also as a function of the part geometry, the parameters required to achieve desired melt pool characteristics will also be a function of geometry. The geometry of the melt pool is important as its width and depth can affect part density and its length can affect the microstructure through the cooling rate.

In current powder bed fusion systems, geometry-specific parameters can be entered for geometries such as the core, skin, and downward-facing surfaces. But, achieving controlled melt pool characteristics throughout a part requires voxel-by-voxel control of the parameters [10]. In situ sensors and feedback schemes could aid such control. The high laser energy and speeds involved in metal powder bed fusion fast transition states. The responses time of the melt pool are consequently fast. Achieving optimized input parameters linked to in-situ analysis is referred to as an “intelligent feed forward” control [11]. Modeling and simulation combined with high-performance computing optimization (solving the inverse problem) have the potential to provide the next step in such voxel-by-voxel control of the process.

AM process parameters are the input and primarily determine the rate of energy delivered to the surface of the powder and how that energy interacts with the powder. Process signatures are dynamic characteristics of the powder heating, melting and solidification processes as they occur during the build. They can be observable or derived. Product qualities are associated to previous information. They should facilitate the development of the in-process sensing and product qualities. The objectives followed in this document are to identify those correlations between process parameters, process signatures and product qualities to exploit these relationships in the monitoring and control solutions. Current in-situ analysis systems to automated in-process detection and control of defaults are reviewed. Sensors are detailed and new strategies are proposed using the Open-architecture pLatform for Laser pOwder bed fusion and in-Process Analysis: OLLOPA.

3 Laser powder bed fusion – physic aspects

The selective laser melting process includes a variety of physical effects with huge disparities in temporal and spatial scales, making comprehensive, first-principles modeling practically impossible. However, the disparity in scales enables the use of simplified models for some aspects of the process. A simulation at the scale of the powder would consider the laser interaction with the powder, powder melting, and evolution of the melt pool. A simulation at the scale of the part would take into account laser heating and melting treated as a thermal source, part shape, and laser scan strategies and would be able to calculate the residual stresses. The ranges of applicability of the simulations can overlap, opening the possibility for the mutual code validation.

3.1 Powder absorptivity

An important component of metal additive manufacturing process modeling efforts is the description of the absorption of laser light by the metal powder and the spatial distribution of

the absorbed energy. Direct measurements of the absorption are quite difficult due to multiple-scattering [12]. Also it is problematic to make use of measurements obtained without detailed specifications of the experiment, since the absorption depends on the powder material, the distribution of particle sizes, the spatial distribution of the particles, and the laser beam size and profile. Thus, it is not sufficient to know only the results for one particular powder of a given material and for a particular beam. Similarly, the spatial distribution of absorbed energy is difficult to obtain experimentally. These considerations reinforce the usefulness of absorption calculations. Powder absorptivity need to be clarified using refractometry evaluation for different powder granulometry and spatial distribution.

However, a commonly used laser absorption model proposed by Gusarov et al. [12] assumes diffusive radiation transport in the powder and it was demonstrated a deviation with experimental evaluation. The model can be applicable to a ceramic powder or to a thick, high-porosity metal powder. This assumption, however, is not applicable for the thin (a few powder particles thick), low-porosity metal powder layers used in the selective laser-melting process. In this case most of the energy is absorbed at the surface of the top layer, and the absorption is highly non-uniform even on the scale of individual powder particles [13]. So, the laser deposits the energy on the surface of the particles. The energy and material inputs in the melt pool change dynamically during the process. Several researches investigated the causes and consequences of the fluctuations.

Rubenchick et al. [14] were interested in not only the total absorbed power but also the spatial distribution of the absorbed power. In some additive manufacturing machines, the laser beam size is roughly comparable to the powder particle size. Figure 2 shows the distribution of absorbed irradiance along the top layer of an array of stainless steel spheres as the beam is rapidly scanned across the array. This distribution was obtained by calculating the absorbed irradiance pattern at a number of points along the path and plotting the sum as a function of position. It gives a qualitative picture of the absorbed irradiance on a short time scale compared to thermal times, i.e., for a sufficiently fast scanning speed. This figure highlights that the scattered light is well confined and that the typical absorption area is comparable to the beam area.

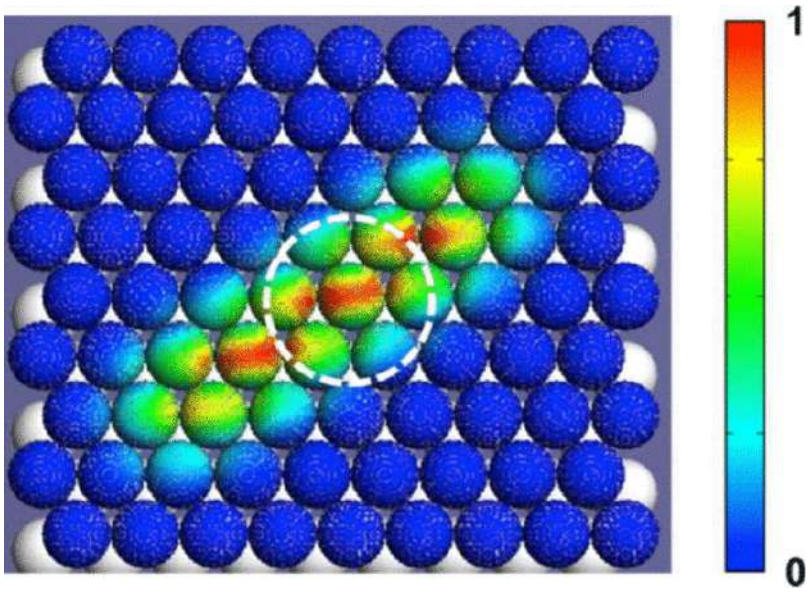

Figure 2: Irradiances for 61 successive beam positions from left to the right in steps of 2 µm [10]

Real powder is different from the monosized powder considered above. A realistic powder has a distribution of sizes and a non-uniform geometrical arrangement, generally with porosity greater than that of an ideal array. Absorptivity deviation was evidenced depending on the powder granulometry [14]. The results are summarized in Table 1, which demonstrates that a change in the powder structure can noticeably affect the absorptivity. For a moderately absorbing metal such as stainless steel, the difference is not significant, about a few percent. As a consequence, the absorptivity of the stainless steel and titanium are not very sensitive to powder structure and powder feed system. On the other hand, for highly reflective metals such as silver and gold, the variation can be nearly a factor of two. In these cases, multiple scattering is very important, and the powder configuration and size distribution affect the total absorptivity.

Table 1: Absorptivity calculated for a number of materials and three granulometry configuration [14]

Material	Mono array	Gaussian array	Bimodal array
Al	0.22	0.18	0.24
Ti	0.64	0.62	0.66
SS	0.60	0.58	0.63

There are many reasons to proceed direct absorptivity measurements, even in the presence of detailed absorptivity simulations: the powder particle shape can differ from ideal spheres, the real powder structure in an experiment can differ from that produced by

the numerical model, surface oxides can affect the absorptivity, and the refractive index of the alloy materials can be very different from the pure metal measurements. As an example, the Al absorptivity for 1 µm light according to Palik [15] is about 5%. The real measurements of the bulk Al gives absorptivity about 20% for manufactured parts. This is partially explained by the effect of the oxide layer and partially by the surface roughness. As a result, there is increasing demand for a simple compact system for fast measurements of the temperature-dependence of the laser absorptivity up to and including the molten state. Measurements were done for Ti-6Al-4V and Aluminum alloys powder.

During laser-powder bed interactions, a part of the laser radiation is reflected and the rests of the laser light is absorbed by the powder layer. An Ulbricht sphere is used (Figure 3). A substrate covered with a powder bed layer is introduced inside the sphere. A laser irradiation is then applied on the powder bed during a time *t0* during which the reflected part of the beam is distributed throughout the inner walls of the sphere and detected by a photodiode. A voltage versus time signal is then recorded with the amplitude proportional to the reflected energy. The reflectivity is obtained by considering the ratio between the voltage amplitude recorded on the powder bed and the reference voltage (obtained with a mirror). A technical note is dedicated to those experiments.

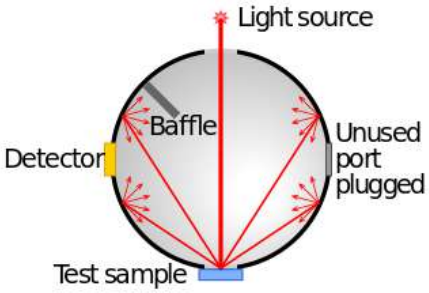

Figure 3: Basic principle of Ulbricht sphere

It was demonstrated that due to multiple scattering the powder absorptivity is greatly increased in comparison to flat surface absorptivity. Several materials were studied (Figure 4). The absorption for the metals with high absorptivity (TA6V) is practically independent of powder structure. The insensitivity of absorption to the powder structure may explain the independence of Ti-6Al-4V absorption on powder type. The absorptivity value for Ti alloy in our measurements is about 65%, somewhat higher than predicted by the modeling value ~62%. One possible explanation is that the calculations used the refractive index for the pure Ti, which can differ from that of Ti-6Al-4V. Also two powder granulometry were studied experimentally and a variation of 3-4% was evaluated. The powder size and granulometry do not influenced clearly the absorptivity.

Calculated values for Al alloy are very different from the measurements. They suggest that the oxide layer and the structure of the surface are important. For a flat surface, the observed absorptivity of Al is over 18% for 1.07 µm light, much higher than the 5% value predicted using the textbook refractive index. The increase in powder absorptivity in comparison with a solid material is consistent (54%). It was also demonstrated an impact of the particle sizes and the granulometry. However alloys chemistry changed the absorptivity corresponding to wrought series.

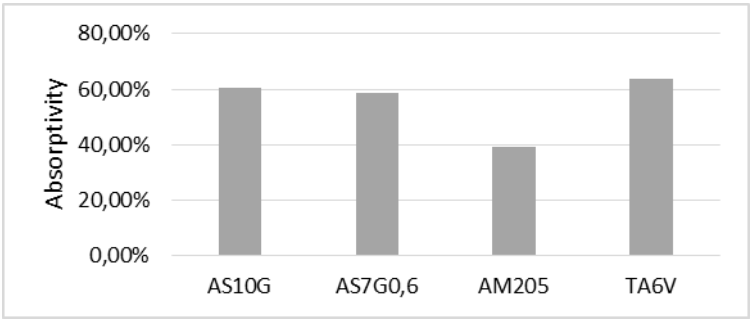

Figure 4: Measured absorptivity data for AS10G, AS7G0.6, AM205 and TA6V

The previous study was static. The values are the means of 5 measurements. However, similar analyses were performed in dynamics. The powder bed moved linearly at 100 mm/s below a laser source and the reflectivity measurement was continuously performed. It can be observed that reflectivity changed depending on the powder bed density. Those variations could explain the deviation of the energy density over time. This clearly indicates that in-situ analyses at the powder scale are required to evaluate state variable. Those results will be published by R.KROMER et al.

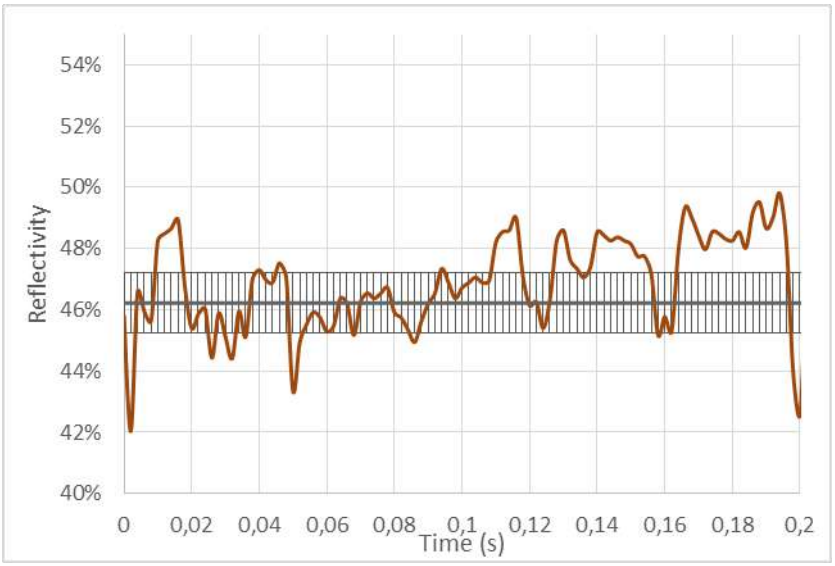

Figure 5: Reflectivity measurement versus time of aluminum alloy

3.2 Melt-pool and solidification

So, the laser-powder interaction starts with a random powder layer on a substrate. The powder particles rapidly melt and begin to consolidate well within the laser beam spot. Fast process characterization is required to dynamically follow the melt pool evolution. For optimal processing conditions, the laser beam must melt the powder layer and some depth of substrate to provide good bonding of the new layer. When the laser interacts with the powder particles, the particles are practically thermally isolated from each other and the melting is rapid. When the laser starts to melt the substrate, the thermal conduction losses through the substrate slow down the melting rate. In an optimal processing regime, the substrate under the laser spot will be melted to a depth comparable with the thickness of the new layer. From the above arguments it follows that in the optimal regime, the powder particles must be melted near the leading edge of the laser spot. Another effect is the interaction of the laser with the evaporated plume. It is usually assumed that for intensities below 100 MW/cm² the laser absorption in the evaporated plume and laser-produced plasma is unimportant [17]. While the vapor produced as a result of this interaction, it can be useful as the diagnostic tool; it can reflect the energy balance.

One of the primary drivers for consolidation of the melted particles and subsequent motion of the melt pool is surface tension. Based on information on the surface locations in adjoining elements, local curvature of the metal pool surface changes. It is also dependent on the temperature. Marangoni convection is driven by the surface temperature gradient between regions of high and low temperature on the surface of the melt pool. For many materials, surface tension decreases as the temperature increases, leading to a flow away from the melt surface closest to the laser spot. Other drivers of melt-flow motion are the inflow of newly melted material and curvature-driven surface tension. The Plateau-Raleigh instability in a long, cylindrical melt bead can cause a pinching-off of some sections of the pool from others. The strong curvature of the melt pool near the laser spot draws melt flow back into this region. The thermal gradient evolution can be correlated to the melt-pool morphology, as it is demonstrated by Rosenthal's law. Specific evaluation at the melt-pool scale is required and specifically at high frequency. The laser spot moves at around 1m/s.

Then, melt pool must solidify due to heat loss. One primary loss mechanism is thermal conduction, largely to the substrate. Another mechanism is the conduction through the adjacent powder bed, though this effect is limited by the poor effective thermal conductivity of the bed, only about an order of magnitude higher than the gas used as the backfill atmosphere. A thermal radiation loss could also be suggested. The total energy loss needs also to include the evaporation. Phase transitions are considered entropic.

Evaporation of metal, particularly under the intense laser spot, is an important part of the dynamics and energy balance of the SLM process, because the mass loss is expected to be small and the processes are dominated by very near-surface effects. The two effects are the vaporization energy loss and the recoil pressure that balances the momentum of the departing vapor [18]. Laser-plasma interactions and the subsequent re-radiation of energy deposited in the plasma back to the work piece need to be studied. Experimental work has indicated that a mode of SLM processing that approaches the keyhole regime is not advantageous to build quality.

Those effects are linked directly to instabilities or not-well evaluated mechanisms during the laser-matter interaction. They are related to the defaults formation [19]. The different defects are listed below. However, several aspects are not linked to controllable parameters. Measurements are hence required for real-time analysis of laser powder bed fusion processing at the melt pool scale and time. Self-learning aspects with meta-model will be developed with the correlation suggestion details later on.

3.3 Categories of defects and their causes

Olakanni et al. proposed different defects which originate during the process [20]. Understanding the defects and their causes represents the first step to design process monitoring and control tools before being able to envisage and develop a dedicated strategy. Porosity is particularly critical for most metal AM applications. It impacts strongly the fatigue performance and the crack growth characteristics. It consists of voids inside the bulk of the fused material [21]. Those voids can be found:

- Within the layer. Spherical and non-spherical pores can be observed. Their sizes is nearly microns;
- Between adjacent layers. The pores are acicular and elongated. Their sizes are more than 50 µm in length. Mainly located in the hatching areas and the external border;
- On the external surface. It defines the pores located near the border.

More common pores are found within the layer, and they may have different size, shapes and spatial distributions. The voids observed between the layers are referred to as ‘acicular pores’ and they are characterized by an elongated shape [23]. The pores may be either spread inside the bulk or located mainly between the internal hatching area and the external border (under-skin pores). Pores maybe found on the external surface as well.

Residual stresses in SLM have been pointed out to arise from two different mechanisms [24], including the thermal gradient mechanism and the cool-down phase of molten top layers. As a consequence of a stress relief through fracturing when the tensile stress exceeds the ultimate tensile strength of the solid material at a given point and temperature, cracking phenomena occur.

Melt ball formation can be responsible of those effects [22]. It occurs when the molten material solidifies into spheres instead of solid layers, which is a severe impediment to interlayer connection. Surface tension drives this phenomenon. It could increase the discontinuity of the interlayer creating pores or protrude powder deposition.

LPBF processes involve highly localized high-heat inputs during very short beam-material interaction times that will therefore significantly affect the microstructure of the part. Microstructural inhomogeneities or non-equilibrium microstructures, together with above mentioned defects, may have a detrimental effect on the mechanical and functional performances of the part.

The above defects are responsible of the macroscopic mechanical properties of the part. The objective is then to determine the process parameters responsible of those defects generation. This study, by gathering in a detailed discussion, information about defect generation mechanisms, aims at identifying a representative physical quantity that can be measured during the process and the corresponding in-situ sensing equipment.

4 Measurements

As mentioned, quality of the parts resulting from LPBF processes varies significantly and depends on many interrelated influencing factors such as powder characteristics, process parameters, geometry and surrounding conditions.

4.1 Pre-process

Pre-process measurements are generally not directly applicable to in-situ feedback control. However, they can potentially be used to define appropriate system input parameters, or supplement a process model for use in feed-forward control. They are also crucial in establishing relationships between input process parameters and process and part characteristics. These measurements often relate to material properties (density, thermal conductivity, etc.) and intrinsic properties of the system (laser power, powder absorptivity, etc.). Kruth et al. provided a list, based on a literature review, of additional material related properties that significantly affect melt-pool signatures: surface tension, viscosity, wetting, thermo-capillarity effects, evaporation, and oxidation [25].

Researchers at the National Institute of Standards and Technology (NIST) summarized metal powder characterization methods, in particular those that measure and describe powder size and distribution [26]. Another NIST study measured size distribution, particle morphology, chemistry, and density of powders and compared sample-to-sample consistency and variability from recycling of used metal powders [27]. Amado et al. also reviewed and demonstrated multiple methods of flowability characterization for polymer LPBF powders for SLS applications [28]. While these works thoroughly described powder characterization techniques, they did not investigate the relationships between variations in these characteristics and resulting process signatures or final part quality. Laser powder reflectivity investigations are then developed in the study using blue wave laser. It will be possible to measure the spatial distribution of powder bed density. It could be then used as process input.

The role of powder size and size distribution in sintering kinetics is well understood, i.e., it affects the relative density of the powder, which, in turn, affects the activation energy required for heated particles to coalesce [29]. Smaller powder sizes with higher relative powder densities require less energy to sinter. It is known that a wider distribution of particles sizes can allow for higher powder density, since smaller particles can fit in the gaps between larger particles.

High relative densities increase the relative thermal conductivity of the powder bed. However, this decreases the absorptivity of the laser energy in AM systems, counteracting the benefits of a lowered energy barrier [30]. In some instances, these effects may negate each other. Spierings et al. showed that unless a certain relative powder density is achieved, a lower scan speed (e.g., higher energy density) is required to produce fully dense parts [31]. Differences in the relation of the powders to the densities, the layer thicknesses, and laser scan speeds indicate that powder grain size distribution should be taken into account for optimal results.

Further, local thermal conductivity has an effect on melt-pool signatures and thus part quality. Although metal powder thermal conductivity has been measured in multiple instances [32], conductivity of the fully dense material is generally better known and easier to measure. This measurement can be supplemented to models to derive the effective powder conductivity.

Finally, there are certain pre-process measurements not involving input materials. For example, some part quality issues may stem from machine errors. These may include motion and positioning errors (with well-established measurement guidelines that may be taken from machine tool standards, e.g., ISO 230-1), or errors in the laser optics and

scanning system. These error sources and solutions for increased precision through better design or feedback control are not unique to AM, but relevant also to other manufacturing processes.

4.2 In-process measurements

The primary focus of research in in-process monitoring has been associated with determining the geometry and the temperature profile of the HAZ. IR thermography and pyrometer are two well-developed non-intrusive techniques for the measurement of surface temperatures. There is also some reported work on the in-process monitoring of the dimensional accuracy, errors, and defects during the build process.

Thermographic imaging of AM processes can be grouped based on the optical path used by the imaging system. In co-axial systems, the imager field of view aligns with the laser beam through the beam scanning optics. In these systems, the field of view follows the melt-pool throughout its scan trajectory. Alternatively, the imager may be set externally to the build chamber to view the build through a window. An improvised method was developed by Berumenn et al. [33]. Using the co-axial system, they mapped the charge-coupled device (CCD) camera and photo detector signals stemming from the melt-pool in the build plane using the XY laser scan coordinates. This created mapped images of the entire build area, with more local and detailed signatures of the melt-pool. Through this method, they could detect part deformation and overheating near overhanging structures through measured changes in the photo-detector signal. A lower signal resulted from the laser defocusing on distorted surfaces. A higher signal resulted on overhang surfaces that had less heat sinking support structure, and thereby poorer surface quality.

There are several known difficulties with thermography of additive processes. First and foremost, the imaged object's emissivity must be known in order to determine a true thermodynamic temperature from radiation-based measurements. Emissivity is likely different for the melt-pool, unconsolidated powder, and solidified surface, so a thermal image composed of all three components could give deceptive temperature predictions. For example, Dinwiddle et al. noted that the powder areas surrounding the solidified part surfaces glowed brighter than the part in thermal images even though the powder was likely at lower temperature [34]. This was attributed to the lower emissivity of the part surface, which reduced the imaged radiant intensity in these areas. Several techniques have been used to determine emissivity of different build components in AM systems:

1) assume a certain imaged area is at the liquidus or solidus temperature of the melt and use this as a reference emissivity,

2) create an emissivity reference by building and imaging a blackbody cavity,

3) only provide temperature without correction for emissivity (e.g., apparent or brightness temperature) or provide raw sensor signal values.

Another challenge, in particular with co-axial systems, is that f-theta lenses used in scanning systems induce chromatic or spectral aberrations. This requires that only radiation sensor systems with narrow bandwidth near that designed for the f-theta lens may be used accurately. Finally, metallic debris from the HAZ can coat a window or viewport used in an AM imaging system, and disturb temperature measurements by changing the radiation transmission through the window.

Several studies using thermography are of particular interest in relating process signatures to either input parameters or product qualities. Krauss et al. described the radiance (not temperature) images of the HAZ, captured by a micro-bolometer, in terms of area, circularity, and aspect ratio [35]. They compared these measures versus scan speed, laser power, hatch distance, scan vector length, layer thickness, and changes when the melt-pool passes over an artificial flaw. Despite the relatively slow exposure time and limited resolution, they showed that size of the HAZ area was the most suitable measures to detect deviations in scan velocity or laser power.

Yadroitsev et al. noted how melt-pool temperature, width, and depth in single track scans in Selective Laser Melting (SLM) of Ti-6Al-4V increased with laser power and ‘irradiance time’, defined as the ratio of laser spot diameter by scanning speed [36]. Peak melt temperature increased with both power and irradiance time, but was more sensitive to power over the ranges measured. Melt-pool width and depth were measured from cross-sections cut from the melted tracks. They thoroughly characterized the microstructure of the SLM material for two scan strategies, and multiple post-build heat treatments. However, no definitive comparison of microstructure to the SLM process parameters or the thermal measurements was highlighted.

Hofmeister et al. empirically correlated cooling rate behind the melt-pool to the melt-pool size and noted how these changed depending on proximity to the build substrate and thus local average thermal conductivity [37]. They also noted calculating cooling rate is more difficult in a real-time monitoring system, and measuring melt-pool length as a corollary signature is more feasible.

Santosprito et al. describe a thermography based system to record the heat movement through the laser track [38]. Since defects (cracks, porosity, etc.) create lower conductivity regions and affect heat flow, they can be detected using thermography. However, since the

changes due to these defects are small, they created new algorithms such as asymmetrical spatial derivative analysis, asymmetrical time derivative analysis, and asymmetrical line profile analysis (using multiple image frames and image subtraction) to improve the effectiveness of the defect detection. It was reported that a minimum defect size around 400 µm is detectable with this system.

Dinwiddie et al. developed a high speed IR thermographic imaging system with an integration time of 1.0 ms, retrofitted to a commercial electron beam machine, to monitor beam-powder interaction, quantify beam focus size, and detect porosity [39]. To overcome the contamination of the optics due to free metal ions released during the process, they designed a shutterless viewing system allowing continuous IR imaging of the beam-powder interaction. The paper describes the design of the system as well as examples of how to use this system in e-beam focus measurement (which requires spatial calibration), detection of over-melting during preheat, and porosity detection. However, since there was no temperature calibration, the images could not be converted to true temperatures.

Pavlov et al. described pyrometric measurements taken co-axially with the laser to monitor the temperature of the laser impact zone to detect deviations of process signatures that correlate to deviations of process parameters from their set values [40]. This approach relies on the sensitivity of the temperature of HAZ with respect to process parameters. The laser impact zone surface temperature was measured using a bi-color pyrometer (1.26 µm and 1.4 µm wavelengths with 100 nm bandwidth) covering a circular area of 560 µm diameter with 50 ms sampling time. A laser spot size of 70 µm diameter results in about a 100 µm re-melted powder track. A 400 µm diameter optical fiber was used to collect temperature information. Temperature was represented as digital signal levels. Using this system, they investigated three strategies, namely: time variance of pyrometer signal during laser scanning of multiple tracks, changes in pyrometer signal as a function of hatch spacing (with thin and thick powder layers), and pyrometer signal changes as a function of layer thickness. The authors used this measurement method to differentiate the three process strategies proposed. They found that the pyrometer signal from the laser impact zone is sensitive to the variation of the main operational parameters (powder layer thickness, hatch distance between consecutive laser beam passes, scanning velocity, etc.), and could be used for on-line control of manufacturing quality.

Bidare et al. reported the design of a metal powder bed fusion system for in-situ monitoring of the build process during additive manufacture [41]. Its open-architecture design was originally determined to enable access for X-Rays to the melt pool, but it also provides access to the build area for a range of other in-situ measurement techniques. The system is

sufficiently automated to enable single tracks and high-density, multiple layer components to be built. It is easily transportable to enable measurements at different measurement facilities and its modular design enables straightforward modification for the specific measurements being made. They demonstrate that the system produces components with >99% density. Hence the build conditions are representative to observe process fundamentals and to develop process control strategies.

4.3 Post-process

The effects of various process parameters on part density for many materials have been investigated and the contributors causing porosity have been identified. Laser power, scan speed, scan spacing, and layer thickness can be directly related to energy density and thus to part density. Several researchers have studied the effects of energy density parameters on different materials like 316L stainless steel [42], 17-4 Precipitation Hardening (PH) steel [43], Ti6Al4V [44], AlSi7Mg [45] and (AISI)-630 steel [46]. Their efforts suggest a correlation between the energy density and the part density. Parthasarathy evaluated the effects of powder particle size, shape, and distribution on the porosity of 316L stainless steel [47]. Porosity/density has a direct effect on the mechanical properties of components fabricated by LPBF [48]. Internal and external pores, voids, and micro-cracks introduced during fabrication act as stress concentrators that cause premature failure and thus compromising part quality.

5 Parameters, signatures and qualities

As summarized in the previous sections, the influence of AM process parameters on the resultant part quality in general has been widely studied and reported. To establish foundations for process control, sub-category of the process parameters, process signatures and product quality according to the abilities to be measured and/or controlled are set. Process parameters are inputs to the LPBF process and they are either potentially controllable or predefined. Controllable parameters (e.g., laser and scanning parameters, layer thickness, and temperature) are used to control the heating, melting, and solidification process and thus control the part quality. Predefined parameters, for example, include part geometry, material, and build plate parameters. Controllable process parameters generally correlate to the observable and derived process signatures (e.g., melt-pool size, temperature, porosity, or residual stress). Derivable parameters cannot be directly measured but can be calculated with a numerical model, such as the maximum depth of a melt-pool. For purposes of correlations we further subdivide the process signatures into three categories namely: melt-pool, track, and layer. Process signatures determine the final product qualities (geometric, mechanical, and physical). Developing correlations between

the controllable process parameters and process signatures should support feed forward and feedback control, with the goal of embedding process knowledge into future control schemes. The Figure below categorizes and lists the process parameters, process signatures, and product qualities to derive needed correlations.

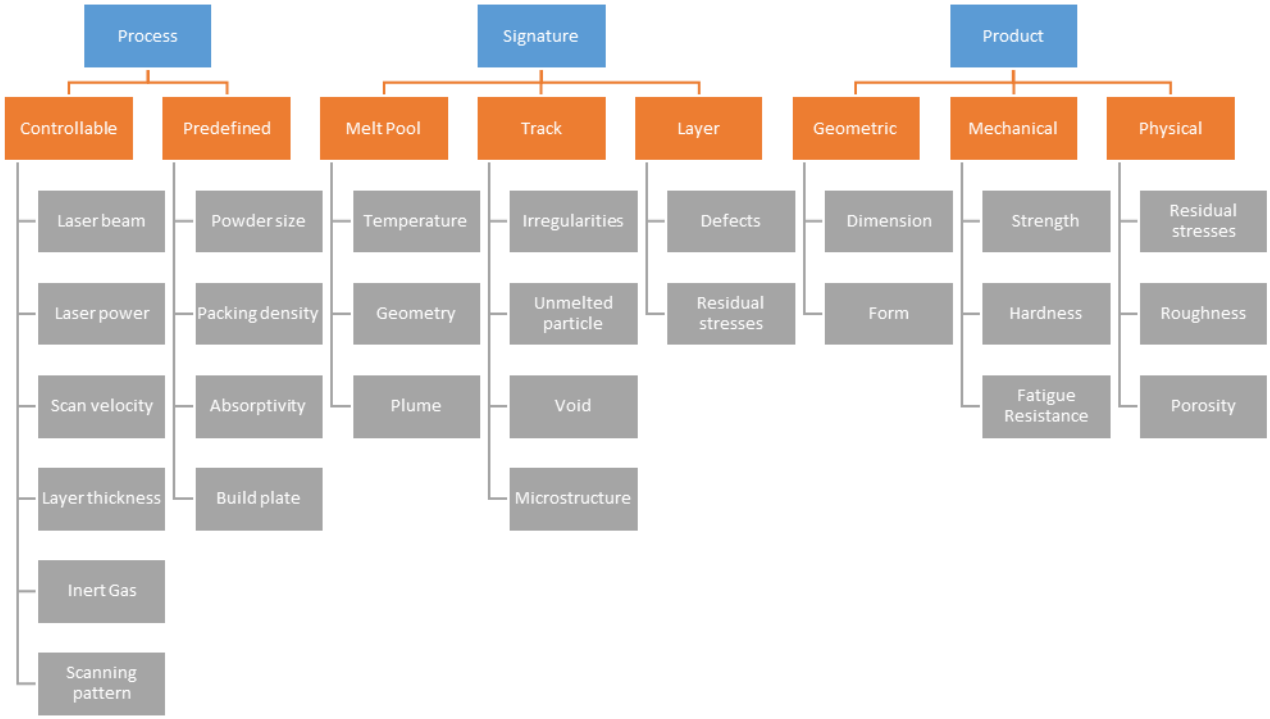

Figure 6 : Laser beam melting process parameters – laser-powder interaction signatures – product properties

The main process controllable parameters include the following:

1. Laser Beam Velocity: quantifies the scanning speed and direction of the laser beam.
2. Laser Power: quantifies the power of the laser beam.
3. Laser Beam Diameter: quantifies the diameter of the laser beam scanning the powder bed.
4. Layer Thickness Variation: quantifies the variation to the preset powder layer thickness for refilling the previously fabricated sub-layer.
5. Inert Gas Flow: quantifies the inert gas flowing above the powder bed for cooling using two sub-parameters namely the Flow Rate and the Flow Pattern, such as laminar flow, turbulent flow, or transient flow, of the inert gas.
6. Scanning Pattern: quantifies the order of the scanning directions of the laser beam.

Predefined process parameters are those process-related parameters that are defined prior to laser scanning and cannot be changed during scanning. The following are the predefined parameters:

1. Powder Size Distribution: quantifies the particle size distribution of the metal powder.
2. Layer Thickness: quantifies the predetermined thickness of powder layer for each layer of scanning.
3. Packing Density: quantifies the density of powder in the powder chamber after packing.
4. Absorptivity: quantifies the coefficient of the heat absorbed per unit mass of powder.
5. Reflectance: quantifies the ratio of the heat reflected by the powder bed to the heat delivered by the laser beam.
6. Build Plate: indicates the type of plate that is used to fabricate a product.

Melt-pool, a subcategory of process signature, has the following parameters:

1. Temperature: includes two sub-parameters namely the Maximum Temperature of the melt-pool, and the Temperature Gradient of the melt-pool.
2. Geometry: includes three sub-parameters namely Maximum Width of the melt-pool, Maximum Depth of the melt-pool, and Length of the melt-pool behind the maximum width.
3. Plume Characteristic: characterizes the plume.

Track, another subcategory of process signature, has the following parameters:

1. Geometric Irregularity: indicates irregularities in the track (e.g., balling, voids, discontinuity, and delamination) causing the fabricated track to deviate from the desired track.
2. Unmelted Particle: indicates the location of an unmelted particle in the track.
3. Shrinkage: indicates the size reduction due to cooling and solidification of the track.
4. Residual Stress: quantifies residual stress in the track due to shrinkage or deformation, such as bending and twisting.

5. Microstructure: indicates microstructure of the track denoted using two sub-parameters namely Crystal Structure (including grain size and grain growth direction) and Metal Phase.

6. Void: indicates the location and shape of an empty space, such as pore, crack, and delamination, in the track.

Layer, the other subcategory of process signature, has the following parameters:

1. Geometric Irregularities: indicates irregularities in the layer. Combined shape irregularities from all the tracks in a layer can make the entire fabricated layer to deviate in shape.

2. Residual Stresses: indicates the residual stresses and stress distribution in the layer.

3. Unmelted Particles: indicates particles, which are not melted by the laser beam, in the layer.

4. Voids: quantifies empty spaces, such as pores, cracks, and delamination, in the layer.

5. Microstructure: indicates the crystal structures and metal phase in the layer.

6. Defects: quantifies imperfections (e.g., delamination, discontinuity, and severe deformation) in the layer such that the product can be disqualified if the defect cannot be remedied in fabricating the succeeding layers.

The category of Product includes the following:

1. Dimensional deviation: quantifies the deviation of the measured dimension from the nominal dimension due to form and size errors.

2. Mechanical property: quantifies mechanical performance of the product, such as strength, hardness, toughness, and fatigue resistance.

3. Surface Roughness: quantifies the roughness of a surface of the product.

4. Porosity: quantifies the amount of voids in the product.

5. Defects: quantifies imperfections in the product that makes the product fail to perform by design.

6. Residual Stress: quantifies unintended residual stress in the product.

With the parameters individually defined in the previous section, this section describes qualitative correlations to describe the cause-and-effect relationship between process control parameters, process signatures, and product quality. The correlations are synthesized according to literature review in the previous sections. Most reviewed papers discussed the correlations between process parameters and product quality (e.g., increasing laser power can improve product mechanical strength due to deeper and wider melting). Those papers that discussed process signatures mostly focused on melt-pool temperature and area. Process parameters along with signatures in general have not yet been directly related to product quality.

From the literature, process parameters are driving factors that determine a melt-pool formation. The correlations between controllable process parameters and melt-pool signature parameters (Melt-pool Temperature and Melt-pool Geometry) depend on the controllable (Beam Diameter, Beam Power, and Beam Velocity) and predefined parameters (Reflectance, Packing Density, Layer Thickness, Powder Size Distribution, Previous Layer/Substrate, and Build Plate). Plume Characteristic generally depends on the Beam Diameter, Beam Power, Beam Velocity, Scanning Strategy, and Inert Gas Flow (including flow rate flow pattern).

After the melt-pool cools, the metal solidifies and forms a track. Shrinkage depends on the controllable process parameters namely the Layer Thickness Variation and Powder Packing Density. The thicker the layer, the more the metal shrinks. The higher the powder packing density, the less the metal shrinks. The Geometric Irregularity depends on Melt-pool Temperature, Melt-pool Geometry, Shrinkage, Beam Velocity, and Layer Thickness. If the Melt-pool Temperature is too high, the shape of the track will be wider due to extreme melting. If the Melt-pool Geometry is larger than the desired geometry, the track shape will become too large. Shrinkage deforms the shape of the track from the shape of the powder layer. If the Beam Velocity is too fast, balling occurs and causes Geometric Irregularity in the track.

Voids depend on Melt-pool Geometry, Melt-pool Temperature, and Fabricating Adjacent Track. Similar to Unmelted particles, if the Melt-pool Geometry is irregular, some particles will not have the sufficient heat to melt, and pores will be in the track. Similarly, if the Melt-pool Temperature is lower than the ideal temperature, Unmelted particles can occur because of incomplete melting, and pores will be in the track. Fabricating an adjacent track can remelt the Unmelted particles and, thus, remove Voids.

Microstructure includes dendrites, grain size, grain growing direction, and solid phases and depends on the following melt-pool parameters: Melt-pool Temperature, Temperature

Gradient, Beam Velocity, and Fabricating Adjacent Track. The three parameters i.e., Melt-pool Temperature, Temperature Gradient, and Beam Velocity affect grain sizes, grain growing directions, and metal phases of the track. Fabricating Adjacent Track remelts a portion of the previous track as a heat treatment and thus affects the Microstructure of the track.

The other layer related signatures namely Voids, Microstructures, and Defects. Voids are derived from both the Voids in Tracks and Between Tracks parameter and the Geometric Irregularity parameter. Microstructure depends on the Combined Track Microstructures parameter. Defects depend on the Shape Irregularities, Combined Track Microstructures, Residual Stresses, and Unmelted Particles. Defects indicate the locations, and the types of defects in a layer. If the defects can be remedied in the succeeding layer fabrication, the defects will not be the reason to stop the fabrication process; otherwise, the fabrication process should be stopped to avoid making a product with defects.

For design of AM LPBF process control there must be further development of parameter-signature-quality relationships and relative sensitivities of those relationships through experiments and simulations. Most of the reviewed literature has limited analysis of measurement error and traceability, and there is a need for better measurement uncertainty evaluations and reporting. In such cases, a large uncertainty in a temperature evaluation will result in an uncertainty of the melt-pool size, and therefore inadequate comparison of measurement data with the model output. Better understanding of measurement uncertainty assists system controller design by identifying the necessary level of precision required to attain the goals of the control system. A technological overview are proposed and in-process fault detection and control will be proposed with OLLOPA bench.

6 Technology overview

Melt pool temperature and geometry are the main signature associated to unmelted particle, voids, shrinkage, roughness and residual stresses. The signatures are linked to controllable and predefined parameters which vary in space and time during the process. So, devices to measure a physical value related to the temperature of an object are presented:

- Contact measurement
    1. Thermocouples
    2. Resistance Thermal Detector (RTD)
- Optical pyrometer (non-contact)
    1. Local measurement

- Photodiode
- Bolometer
- Spectrometer

2. Matrix of measurements
    - Thermal camera (visible and IR)

The working principle of a thermal measurement instrument is based on the variation of physical properties depending on the temperature. Two classes of temperature measurement exist: measurements by contact and measurements by radiation. Each of them is pertinent in different cases.

Generally, when localized (punctual) measurements are required, contact measurement is used. It is cheap and easy to setup. However, in special cases the other type is preferred when the studied object is too fragile to support the operation of attaching a sensor to it, or when the object offers a very low thermal capacity the sensor would bias the measurement, or when the object cannot or must not be reached by physical means.

6.1 Contact thermometry

Thermometry is qualified as "contact" when the principal detector is in contact with the object of which the temperature is measured. Several methods exit. Some are qualified "by contact without material link for reading". It means that a substance is applied on the surface of an object which will react to its temperature. The reading is done remotely from this substance. This set of methods includes colorimetry and photoluminescence. These applications are beyond the scope of this synthesis.

The other set of contact methods is qualified as "with a material link for reading". It includes thermal resistance detector and thermocouples.

6.2 Basics

Thermal Resistance Detectors (RTD) use the variation of electric resistance as a function of temperature [42]. Therefore they require electrical current to run through them to create a measurable voltage drop. Also to create an electrical resistance a certain amount of wire is needed which makes them quite bulky. There are two types of RTD. The metallic resistive thermometers which use the following equation as transfer function:

$$R = R_0 + a(T - T_0) + b(T - T_0)^2$$

And thermistances which use the following equation as transfer function:

$$R = a\ exp\left(\frac{b}{T}\right)$$

Thermocouples are defined as a junction between two electrical conductors of different nature. The couple of material creates a thermoelectric potential dependent of the temperature. The electromagnetic force is created by the Seebeck effect which is usually reduced to:

$$u = a\left(T - T_{ref}\right) + b\left(T - T_{ref}\right)^2$$

Thermocouples can be used over a very large range of temperatures from few Kelvins to 1800 K. However thermocouples generate a potential of only few µV which require good quality amplification for measurement.

6.2.1 RTDs

Since an electrical current is necessary to go through the RTD to measure its resistance, there is a systematic bias generated by heat from Joule effect. Depending on the application, this bias must be evaluated to be taken into account in the transfer function. Another source of bias is the length of wire between the RTD and the acquisition electronic card. These wires have their own resistance which must be subtracted to the measurement. Therefore, RTDs are often used in resistance compensating bridges.

They are appropriate to use when a fast response time is not required. Because they are bulky, the response time can be up to several seconds depending on the media. Moreover, they are restricted to small range of temperatures (usually below 200°C). The calibration of metallic resistive thermometers is done at an absolute given temperature (T_0). Consequently, the measurement can be accurate in absolute temperature (providing all precautions are taken care of).

6.2.2 Thermocouples

Several couples of material are used in thermocouples. The most common are listed in Table 2. The choice is mainly made with the maximum temperature required to withstand. Other parameters can become design criteria such as the price or the chemical compatibility.

Thermocouples measure temperature difference between the hot junction (the thermocouple) and the cold junction at the connection of wires to the measuring circuitry

(T_{ref}). Therefore, the cold junction temperature must be known and kept stable or measured continuously to be able to output the proper value of the thermocouple temperature. Usually, thermocouples are used when a high accuracy regarding the absolute temperature is not required.

Table 2: Thermo-electrical couples. Adapted from [43]

Couple	Material (+)	Material (-)	Max Temperature
Type J	Iron	Copper-Nickel (Constantan)	900 °C
Type T	Copper	Copper-Nickel (Constantan)	900 °C
Type E	Nickel-Chrome (Chromel)	Copper-Nickel (Constantan)	900 °C
Type K	Nickel-Chrome (Chromel)	Nickel-Aluminum (Alumel)	1250 °C
Type N	Nickel-Chrome-Silicon	Nickel-Silicon	1250 °C
Type B	Platinum (30%) Rhodium	Platinum (6%) Rhodium	1800 °C
Type R	Platinum (13%) Rhodium	Platinum	1600 °C
Type S	Platinum (10%) Rhodium	Platinum	1600 °C

Thermocouple can be very small, down to 1 µm. At that size, if build with wires, the manufacturing technique is complex and the vulnerability of the thermocouple makes it expensive. To the author knowledge their production is not industrialized. The other possibility to get very thin thermocouple is to manufacture it by metal deposition (process widely used in integrated circuit). It comes with having a thermocouple deposited on a substrate which in some case will be considered as a measurement impediment. The standard manufacturing process (soldering two wires) is in most cases used. This technique can provide thermocouple to the size of 80 µm [44].

6.3 Optical thermometry

6.3.1 Basics

For a black body (theoretical notion), the quantity of thermal energy emitted per second (power) by surface area unit by wavelength (distance) is expressed by Planck's law [45]:

$$M^o_{\lambda,T} = \frac{2\pi hc^2\lambda^{-5}}{\exp\left(\frac{hc}{\lambda k_b T}\right) - 1} = \pi L^o_{\lambda,T}$$

Or by the Wien approximation:

$$M^o_{\lambda,T} = C_1\lambda^{-5}\exp\left(\frac{-C_2}{\lambda T}\right)$$

Thus, a black body outputs its maximum of thermal energy at the wavelength $\lambda_m = 2898/T\ (\mu m)$, 95 % of the energy is emitted in the range of wavelength $[\lambda_m/2, 5\lambda_m]$.

The monochromatic emissivity of a real body is defined as the ratio between the thermal power emitted with the power that would be emitted by the black body at the same temperature at a given wavelength. The total emissivity is defined as the ratio of the integrals of luminance over the full spectrum of wavelength.

$$\varepsilon_{\lambda,T} = \frac{L_{\lambda,T}}{L^o_{\lambda,T}}$$

Figure 7 shows that for metallic material, the emissivity is dependant of the wavelength and the temperature of the material. Figure 7.a shows that the emissivity randomly varies with the wavelength considered.

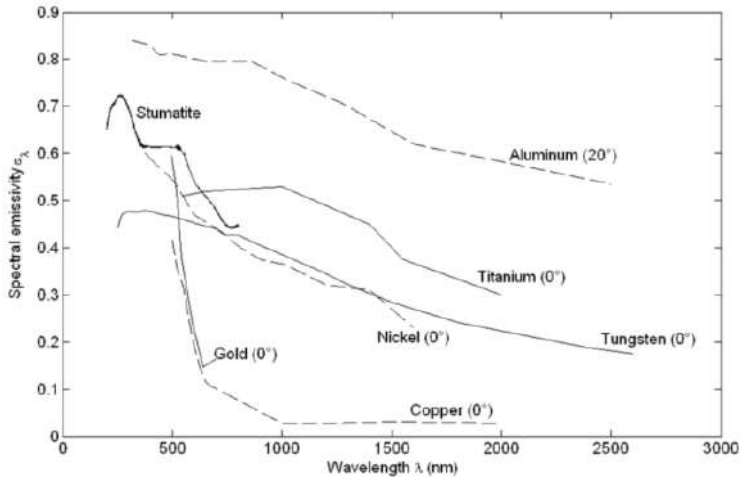

Figure 7: Variation of emissivity of metallic material as a function of wavelength [46]

The approach for temperature measurement can significantly differ from one application to another (see Figure *8*). The choice in the approach implies different set of instruments.

Active pyrometry necessitates an excitation source that passive pyrometry do not require. In this document only passive methods are treated.

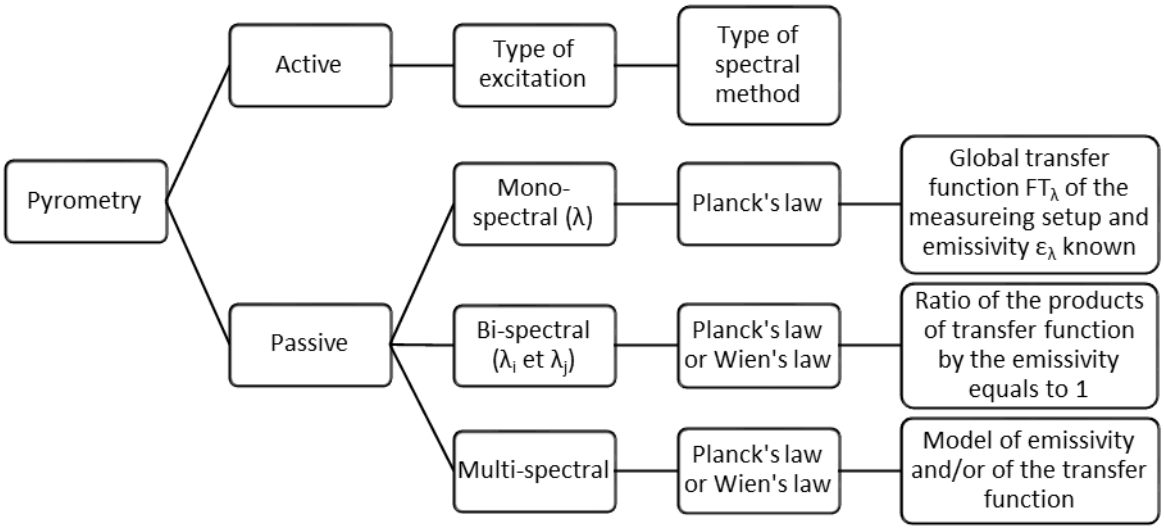

Figure 8: Possible approaches in optical pyrometry [47]

Numerous works showed that optical thermometry is complex to master. The difficulty lies into finding a reliable method that gives the best results (compared to other available methods) independently of the experimental conditions. The problem is that optical temperature measurement is dependent of unknowns such as emissivity and the transfer function of the measuring setup.

To increase the difficulty, the scene of observation is also a source of disturbances. The optical device (camera in **Erreur ! Source du renvoi introuvable.** or an optical pyrometer) is sensitive to the thermal radiation of the observed object but also to the reflection of the environment on the observed object or/and to the background of an object semitransparent. It is also sensitive to the radiation of the atmosphere between the object and the optical device. Inside the optical device, many parts can also interfere with the measurement (lens, sensor, structure, etc).

6.3.2 Mono-spectral approach

Because of the difficulty to have a reliable measurement of the emissivity, certain applications use the temperature of luminance failing to obtain the real temperature. The temperature of luminance is defined as the temperature of the black body at the luminance measured. Thus the real temperature is always higher than the temperature of luminance because from the Wien approximation:

$$\frac{1}{T} = \frac{1}{T_L} + \frac{\lambda}{C_2} ln(\varepsilon_{\lambda,T})$$

This later relation shows that the difference between the real temperature (T) and the temperature of luminance (T_L) decreases with decreasing wavelength. However, Planck's law shows that the emitted energy strongly decreases at wavelength lower than the one of maximum output (λ_m). Therefore, there is a tradeoff to make. Using the temperature of luminance induces inaccuracy because of the bias of not taking into account the emissivity. The inaccuracy tends to zero by increasing the wavelength of observation, but also reduce the amount of energy received by the sensor making the measurement prone to imprecision due to noise measurement.

To increase the accuracy, the emissivity of the material can be evaluated. If applicable, intrusive and direct temperature measurement can be made on the material during calibration. Having signal of the measurement output by the sensor and knowing the true temperature of the material, the total transfer function, including the emissivity, can be computed. Then the total transfer function can be used for temperature measurement.

Finally, in the case of a mono-spectral measurement an optimal wavelength is found to minimize the relative error on the temperature:

$$\lambda_{opt} T = 2410.3\ \mu m.K$$

6.3.3 Bi-spectral approach

The bi-spectral approach allows calculating the surface temperature without knowing beforehand the emissivity when this one is independent of the wavelengths (gray body hypothesis: $\varepsilon_{\lambda_1,T} = \varepsilon_{\lambda_2,T}$). The gray body hypothesis is usually used when the couple of wavelengths are close to each other. It is then assumed that from one wavelength to the other the variation of emissivity can be neglected. In these conditions, the temperature is given by:

$$T = \frac{C_2 \left({}^1/_{\lambda_j} - {}^1/_{\lambda_i} \right)}{ln\left(\frac{M_{\lambda_i}}{M_{\lambda_j}} \left(\frac{\lambda_i}{\lambda_j} \right)^{-5} \right)}$$

This implies that the denominator must not be null. It is found that having a high flux ratio gives temperature measurements that are less prone to error. However, having a high flux ratio usually means working at two wavelengths relatively far from each other with the risk that the gray body hypothesis cannot be applied. The minimal difference of wavelength is defined by:

$$\lambda_j - \lambda_i > \frac{T{\lambda_j}^2}{C_2}$$

Multi-spectral approach is quite different from the two others because it assumes that the emissivity and the transfer function of the acquisition chain are not constant over the wavelengths range that is used. It involves mathematical (polynomial, exponential or fractional) and/or physical (Maxwell, Edwards, Hagen-Rubens or Drude) models and their descriptions are beyond the scope of this synthesis.

6.3.4 Sensor technologies

Two classes of sensor technology exist: the thermal detectors and the quantum ones. The thermal detectors combine (micro) bolometer, pyrometer, thermopile, etc. These devices are sensitive to a wide range of spectrum and do not require to be cooled down. However, as they are based on temperature variation (of the sensor layer) measurement they have a response time somewhat longer than quantum sensors. The quantum sensors include photoemissive, photoconductor and photovoltaic detectors. They have the advantage to be more sensitive and faster than thermal detectors. However they are sensitive on a narrow band of the spectrum (see Figure 9). They are usually chosen depending of the application. Also they require to be cooled down.

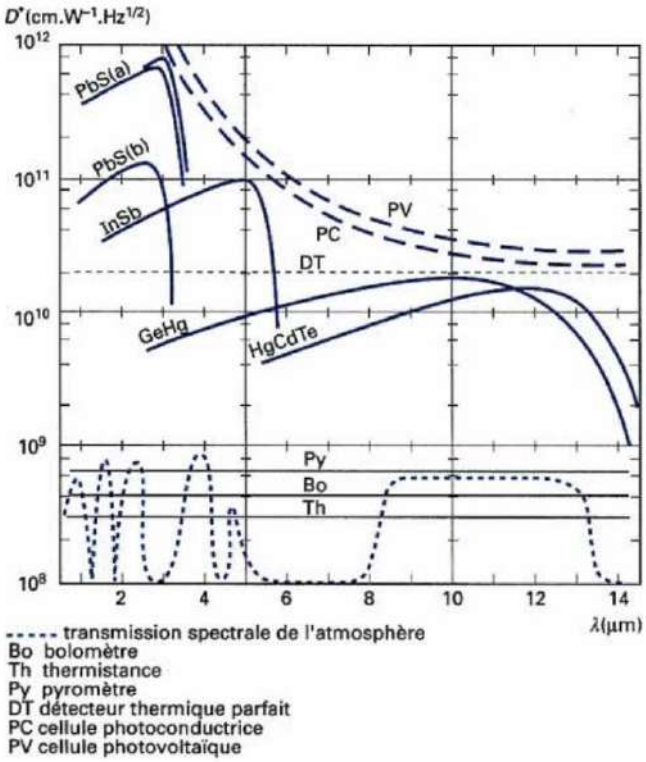

Figure 9: Spectrum sensitivity of sensors [48]

In camera, a matrix of detectors is used. When frame rate is a design criteria with a value over 100 Hz matrixes of microbolometers are not suited. Their response time is too high for such a frame rate. In this case, matrices of quantum detectors are used. However due to their narrow sensitiveness (see Table 3), the detector type should be carefully chosen. Due to their fast response time, the integration time can be very low (typically 1 µs or lower) which enables a direct view of bright object without saturation. So these detectors are also recommended for high temperature observations.

Table 3: Spectrum ranges of some detectors. Data extracted from [49]

Detector	Low	High
InSb	3	5.5
HgCdTe	1.5	5
	4	5
	8	9.5
	8	12
T2SLS	8	9.5
Strained Layer Superlattice	8	12

Regarding single point temperature measurement, such as photodiode based pyrometer, same precautions regarding the choice must be taken.

7 Strategy

However, it is yet unclear which signatures are best modeled or measured, and which input parameters are best controlled for which time scale (either continuously or discrete inter-layer). It is a worthwhile endeavor to create an AM control loop architecture that identifies the multiple potential control loops, and provides a basis for identifying which loops are optimal for controlling which parameter-signature-quality relationship. Finally, several parameters are predefined today. They also vary under the processing. It is necessary to control them too. So major efforts are needed to develop and implement data mining and analysis for automated defect detection, in a statistical process monitoring framework. The signature and their correlation on defects need to be evaluated and rules need to set. Meta-model could be interesting in the development. Two strategies are proposed: energy absorption and melt pool temperature and geometry evaluation.

7.1 Reflectivity

The idea is to look through the scan head to directly observe the laser-matter interaction. The upwards reflect wave lengths from primary optical axis is aligned vertically to the optical buildup of the melt pool monitoring device in which it will reflect on a further mirror through a focusing lens. Finally, beam splitter splits the signals for photodiode 1 and photodiode 2.The front surface of beam splitter 1 transmits the laser wavelength and a proportion of the reflection serves as an input signal for photodiode 3 for a laser power monitoring device

The melt pool monitoring system uses two photodiodes with different dedicated photosensitivity as a function of wavelengths–each is detecting near infrared wavelengths, but the wavelength detected by P1 is different than the wavelength detected by P2. Spectral response is permanently taken up by the individual photodiodes, forwarded to an ADC (analog digital converter) and provided in an FPGA (field programmable gate array). Depending on machine and optical system setup as well as taking into account two different photodiodes the signal to noise ratio is at present up to 10 ns described the reflected portion of the laser wavelength via beam splitter 1 is used as an input signal (measured laser power) of the present laser power (set laser power) by means of photodiode 3. The consumed electric current is converted into an electrical voltage. The measured laser power is then transferred from the LPBM device.

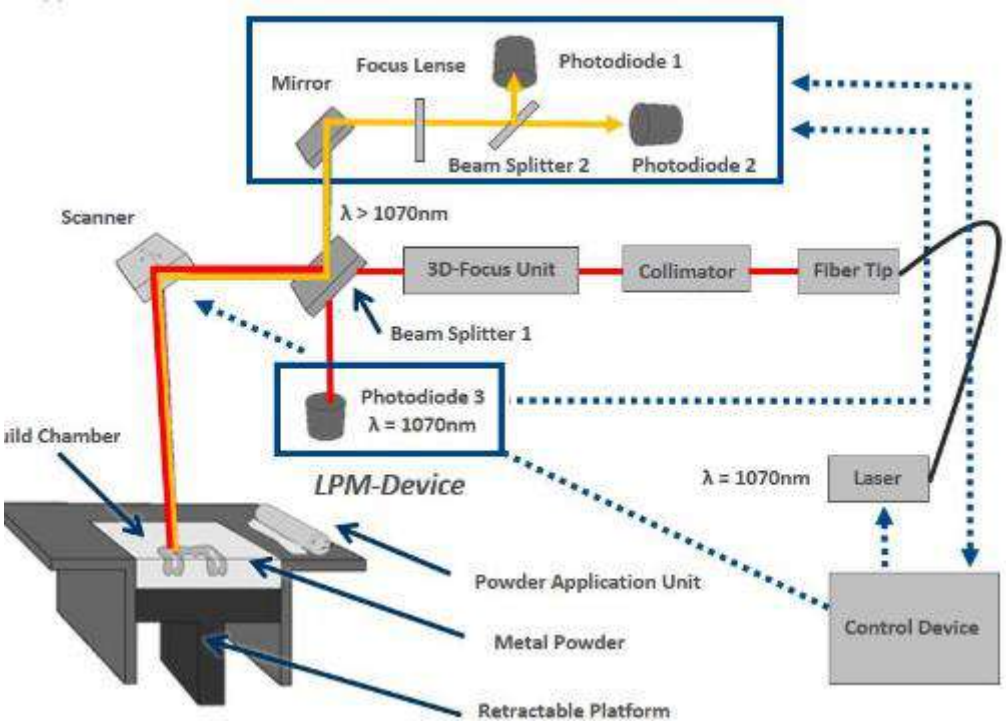

Figure 10: Schematic assembly of optic design with melt pool monitoring and laser power monitoring

7.2 Molten pool

The molten metal emits thermal radiation in a wide spectral band suitable for detectors in the visible and in the infrared band. As the processes under investigation are based on metal powders with melting temperatures at about 1650 °C, thermal radiation can be expected to have a maximum in the near infrared at about 1700 nm. This makes a suitable pyrometer the right choice to measure the thermal emission of the process. Changes in the emission however may have different causes. A change in input energy may lead to the same effect as an increase in powder thickness - both will show an increase in thermal radiation. The same may be true for changes in powder properties or in the case of changed thermal conductivity of the solidified metal beneath the current powder layer. In any of these cases, additional information is necessary to further analyze the operating point of the process. The surface of the powder bed in the vicinity of the interaction point is an additional source of information. Coaxial observation of the illuminated surface provides images that reveal a different behavior of powder particles in the vicinity of the interaction point depending on the thickness of the powder. This behavior can be quantified by image processing and establish a new criterion for mapping events to real process deviations. Finally, this adds to a bijective relationship between measurements and the current process behavior which is necessary to carry out self-optimization on the selective laser melting process. The sensor system of the selective laser melting system uses a coaxial combination of the optical paths

for laser processing and process observation (Figure below). The process observation splits between the infrared spectrum where the thermal emission of the process is detected and the visible imaging spectrum. In the infrared band, a pyrometer is used that is sensitive between 1500 and 1700 nm and provides a time of 10 µs which offers acquisition rates of up to 100 kHz. It is coupled via an optical fiber to avoid direct influences from the machine to the sensor. The camera system is attached on the other side of a beam splitter. The illumination of the surface of the processed layer is provided by laser reflectivity. The major problem with these approaches is that the focus position of the thermal radiation does not coincide with the position of the interaction. There are two types of chromatic errors, axial and lateral aberrations. Axial aberrations lead to different focal positions in the direction of the propagation, resulting in a defocused observation while the processing laser is focused. Lateral aberrations lead to different lateral focus positions for observation and processing wavelength. Usually, both effects overlay, making coaxial observation an ambitious target. Prefocus system is designed to correct the field curvature but it also facilitates a chromatic correction. Lateral errors do not occur at all, since the chief rays of all beams are on the optical axis. Remaining axial aberrations can be corrected using additional lenses in the optical path of the detection system.

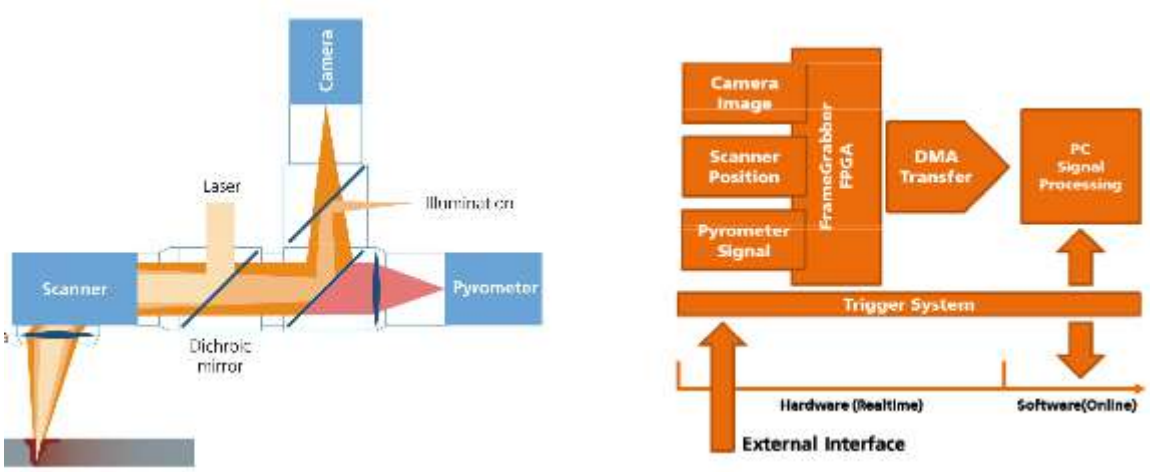

Figure 11: Co-axial system and signal processing

Two possible relative spatial displacements were chosen for the OLLOPA platform to undertake several calibration tests depending on the sensors, the material and the process parameters.

The signal acquisition is realized with an FPGA based hardware that synchronously acquires the camera image, the position information and the pyrometer signal. The data packets are transferred to PC memory for later processing via DMA channels. An external interface is used to control the acquisition on a layer by layer basis.

The trigger system enables active control of the recording process such that each layer can be recorded and stored at the same rate and precision as the manufacturing systems controls the process. The system overall has the advantage, that process observation can be executed at production relevant conditions. The true coaxial observation ensures the precise alignment between processing and observation. The FPGA based synchronous operation of the signal acquisition during the illumination of a layer and in the layer to layer relationship provides information that is reliably aligned. However, data cannot be detailed. The direct visualization is not possible. OLLOPA platform aims also to enable direct observation for data mining strategy.

8 Conclusion

For design of AM LPBF process control there must be further development of parameter-signature-quality relationships and relative sensitivity evaluation through experiments and simulations. Existing control designs are related to melt-pool signature monitoring by varying laser parameters. New traceable methods and identification of new measurable process signatures are in development such as spectral and/or reflectivity measurement. Furthermore, uncertainty evaluations and reporting are required. Meta-model development will assist system controller design by identifying the necessary level of precision and repetition to attain goals of the control process.

Thermal sensors are presented which could enable large scale of measures. Two strategies are also proposed for energy density and melt-pool study. Powder bed evaluation is hence developed to obtain a complete control of the laser-matter interaction. The environment variable will be also evaluated in the process. Finally, the direct visualization of the material behavior will enable a clear overview and propose process maps to organize and communicate the complex, multi-dimensional parameter relationship topology. Multiple potential signatures and control loop strategy will be identified.

9 Reference

[1] ASTM Standard 2792, “Standard terminology for additive manufacturing technologies,” ASTM International West Conchocken, PA, 2012.
[2] H. Yeung, J. Neira, B. Lane, J. Fox, F. Lopez, “Laser path planning and power control strategies for powder bed fusion systems, “Solid Freeform Fabrication 27th , Austin, 2016.
[3] Mellor S., Hao L. and Zhang D;, “Additive manufacturing: a framework for implementation, “ Int. J. Prod. Econ., 149, 194, 2014.
[4] S. Kolossov, E. Boillat, R. Glardon, P. Fisher, M. Locher, “D FE simulation for temperature evolution in the selective laser sintering process.,” Int. J. Mach. Tools Manuf., 42(1), 117, 2004.

[5] M.Mastumoto, M. Shiomi, K. Osakala, F.Abe, “Finite element analysis of single layer forming on metallic powder bed in rapid prototyping by selective laser melting,” Int. J. Mach. Tools MAnuf. 42(1), 61, 2010.
[6] M. Zaeh, G. Branner, “Investigations on residual stresses and deformations in selective laser melting,” Prod Eng., 4(1), 35, 2010
[7] P.Fisher, V. Romano, H.P. Weber, N.P. Karapatis, E. Boillat, R. Glardon, “Laser powder bed fusion additive manufacturing of metals; physics, computational, and materials challenges,” Acta Mater., 51(6), 1651, 2003.
[8] P. O’Regan, P. Prickett, R. Setchi, G. Hankins, N. Jones, “Metal based additive layer manufacturing: variations, correlations, and process control,” Pr. Comp. Sci., 96, 216, 2016.
[9] T. Kimura, T. Nakamoto, “Microstructures and mechanical properties of A356 (AlSi7Mg0.3) aluminum alloy fabricated by selective laser melting, “ Mat. & Design, 89, 1294, 2016.
[10] W.E. King, A.T. Anderson, R.M. Ferencz, N.E. Hodge, C. Kamth, S.A. Khairallah, A.M. Rubenchick, “Laser powder bed fusion additive manufacturing of metals: physics, computational and material challenges, “ App. Phys. Review, 2, 041304, 2015.
[11] S. Clijsters, T. Craeghs, J.P. Kruth, “A priori process parameter adjustment for SLM process optimization,” Phys. Proc., 39, 753, 2012.
[12] A.V. Gusarov, J.P. Kruth, “Modelling of radiation transfer in metallic powders at laser treatment,” Int. J. Heat Mass Transfer, 48(16), 3423, 2005.
[13] C.D. Boley, S.A. Khairallah, A.M. Rubenchick, “Calculation of laser absorption by metal powders in additive manufacturing,” Applied Optics, 2014.
[14] S. Ruchenchik, C.A. Boley, S.C. Mtchell, S.S.Q. Wu, “Metal powder absorptivity: modeling and experiment,” Applied Optics, 2016
[15] E.D. Palik, “Handbook of optical constants of solids,” Academic press, Orlando, 1985
[16] A.V. Gusarov, I. Smurov “Modeling the interaction of laser radiation with powder bed at selective laser melting,” Phys. Proc., 5, 381, 2010
[17] S.I. Anisimov, “*Vaporization of Metal Absorbing*,” Sov. Phys. ,27(1), 182, 1968.
[18] I. Yadroitsev, A. Gusarov, I. Yadroitsava, I. Smurov, « Single track formation in selective laser melting of metal powders, »J. Matter. Process. Technol., 2010, 1624, 2010.
[19] M.J. Matthews, G. Guss, S.A. Khairallahn A.M. Rubenchick, P.J. Depond, W.E. King, “Denudation of metal powder layers in laser powder bed fusion processes,” Acta Mater., 114, 33, 2016.
[20] E.O. Olakanni, R.F. Cochrane, K.W. Dargarno, “A review on selective laser sintering/melting of aluminum alloy powders: processing, microstructure and properties,” Prog. In Mater. Sci., 74, 401, 2015.
[21] S. Everton, M. Hirtsch, P. Stravroulakis, R.K., Leach, A.T. Clare, “Review of in-situ process monitoring and in-situ metrology for metal additive manufacturing,” Mater. And Design, 96, 431, 2016.
[22] X. Zhou, X. Liu, D. Zhang, D. Shen, W. Liu, “Balling phenomena in selective laser melting,” J. Mater. Process Technol., 210, 1624, 2010.
[23] R.J. Smith, M. Hirsch, R. Patel, W. Li, A. Clare, “Spatially resolved acoustic spectroscopy for selective laser melting,” J. Mater. Process. Technol., 236, 93, 2016
[24] J. Mercelis, J.P. Kruth, “Residual stresses in selective laser melting,” Rapid Protyping J., 12, 254, 2006.
[25] J.-P. Kruth, G. Levy, F. Klocke, and T. H. C. Childs, “Consolidation phenomena in laser and powder-bed based layered manufacturing,” CIRP Ann. - Manuf. Technol., 56(2), 730, 2007.
[26] A. Cooke and J. A. Slotwinski, “Properties of metal powders for additive manufacturing: a review of the state of the art of metal powder property testing,” US Department of Commerce, National Institute of Standards and Technology, NISTIR 7873, 2012.

[27] J. A. Slotwinski, E. J. Garboczi, P. E. Stutzman, C. F. Ferraris, S. S. Watson, and M. A. Peltz, “Characterization of metal powders used for additive manufacturing,” J. Res. Natl. Inst. Stand. Technol., 19, 2014.

[28] A. Amado, M. Schmid, G. Levy, and K. Wegener, “Advances in SLS powder characterization,” in Solid Freeform Fabrication Proceedings, 7, 12, 2001.

[29] I. Robertson and G. Schaffer, “Some effects of particle size on the sintering of titanium and a master sintering curve model,” Metall. Mater. Trans. A, 40(8), 1968, 2009.

[30] B. Liu, R. Wildman, C. Tuck, I. Ashcroft, and R. Hague, “Investigation the effect of particle size distribution on processing parameters optimisation in Selective Laser Melting process,” in Solid Freeform Fabrication Proceedings, Austin, 2011.

[31] A. B. Spierings and G. Levy, “Comparison of density of stainless steel 316L parts produced with selective laser melting using different powder grades,” in Solid Freeform Fabrication Proceedings, Austin, 2009,

[32] E. Tsotsas and H. Martin, “Thermal conductivity of packed beds: A review,” Chem. Eng. Process. Process Intensif., 22(1), 19, 1987.

[33] S. Berumen, F. Bechmann, S. Lindner, J.-P. Kruth, and T. Craeghs, “Quality control of laser- and powder bed-based Additive Manufacturing (AM) technologies,” Phys. Procedia, 5, 617, 2010.

[34] R. B. Dinwiddie, V. Kunc, J. M. Lindal, B. Post, R. J. Smith, L. Love, and C. E. Duty, “Infrared imaging of the polymer 3D-printing process,” presented at the SPIE Sensing Technology+ Applications, 910502, 2014.

[35] H. Krauss, C. Eschey, and M. Zaeh, “Thermography for monitoring the selective laser melting process,” in Proceedings of the 23rd Annual International Solid Freeform Fabrication Symposium, Austin, 999, 2012.

[36] I. Yadroitsev, P. Krakhmalev, and I. Yadroitsava, “Selective laser melting of Ti6Al4V alloy for biomedical applications: Temperature monitoring and microstructural evolution,” *J. Alloys Compd.*, 583, 404, 2014.

[37]W. Hofmeister and M. Griffith, “Solidification in direct metal deposition by LENS processing,” *JOM*, 53(9) 30, 2001.

[38] S. P. Santospirito, K. Słyk, B. Luo, R. Łopatka, O. Gilmour, and J. Rudlin, “Detection of defects in laser powder deposition (LPD) components by pulsed laser transient thermography,” 8705, 87050X, 2013.

[39] R. B. Dinwiddie, R. R. Dehoff, P. D. Lloyd, L. E. Lowe, and J. B. Ulrich, “Thermographic in-situ process monitoring of the electron-beam melting technology used in additive manufacturing,” in Proceedings of the SPIE, 8705, 87050K, 2013.

[40] P.Bidare, R.R.J.Maier, R.J.Beck, J.D.Shephard, A.J.Moore, “An open-architecture metal powder bed fusion system for in-situ process measurements,” 16, 1777, 2017

[41] M. Pavlov, M. Doubenskaia, and I. Smurov, “Pyrometric analysis of thermal processes in SLM technology,” Phys. Procedia, 5, 523, 2010.

[42] A.-C. LEGRAND, "Thermographie multispectrale, haute et basse température, application au contrôle non destructif," Ph.D. dissertation, Université de Bourgogne, 2002.[1]

[43] Jean-Pierre BARDON, Bernard CASSAGNE, "Température de surface: Mesure par contact," Techniques de l'Ingénieur, 1998

[44] "Response times," Thermo-electra, available online: https://www.thermo-electra.com/en/producten/technische-informatie/response-times

[45]M. PLANCK, "Ueber das gesetz der energieverteilung im normalspectrum," Annalen der physik, vol. 309, no.3, pp. 553-563.

[46] A.-C. LEGRAND, "Thermographie multispectrale, haute et basse température, application au contrôle non destructif," Ph.D. dissertation, Université de Bourgogne, 2002.

[47] C. RODIET, "Mesure de Température par Méthodes Multi-Spectrales et Caractérisation Thermique de Matériaux Anisotropes par Transformations Intégrales: Aspects Théoriques et Expérimentaux," Ph.D. dissertation, Université de Lorraine, 2014.
[48] François CABANNES, "Température de surface: mesure radiative," Technique de l'Ingénieur, 1996..
[49] "Fast-IR Family" Cooled High-End Scientific Cameras – Telops.